

Pulsed gradient NMR measurements and numerical simulation of flow velocity distribution in sphere packings

L. Lebon,^{a)} L. Oger, J. Leblond, and J. P. Hulin^{b)}

Labo PMMH-ESPCI (URA CNRS No. 857), 10 rue Vauquelin, 75231 Paris Cedex 05, France

N. S. Martys

National Institute of Standards and Technology, Building Materials Division, Gaithersburg, Maryland 20899

L. M. Schwartz

Schlumberger Doll Research Center, Old Quarry Road, Ridgefield, Connecticut 06877-4108

(Received 18 July 1995; accepted 27 October 1995)

The displacement of water molecules associated with the flow of water inside a nonconsolidated packing of 800 μm OD glass spheres has been measured by a pulsed gradient NMR technique. Using a stimulated spin-echo sequence, mean displacements q^f up to 300 μm corresponding to measurement times of up to 200 ms can be analyzed. The measurement can be quantitatively calibrated using the pure molecular self-diffusion of water at zero flow conditions. For molecular displacements much smaller than the pore size, the distribution of the flow velocity component along the mean flow direction is determined at Reynolds numbers high enough so that longitudinal molecular diffusion is negligible. An exponential decay of the probability distribution of the displacements is observed at large distances. The results are very similar to those obtained by numerical solution of the Stokes equation in random sphere packings. At longer displacement distances, a secondary peak of the displacement distribution is observed: It is interpreted as the first step toward the transition toward classical dispersion at displacements much larger than the pore size. The influence of molecular diffusion and of the heterogeneities of the magnetic permeability also are discussed. © 1996 American Institute of Physics. [S1070-6631(96)02802-3]

I. INTRODUCTION

The study of the properties of porous media has often been centered on the determination of macroscopic parameters such as the porosity, the permeability, the electrical conductivity, and the dispersion coefficient. In contrast, studies at the pore scale have until recently been devoted to the analysis of the structure of the pore space and of its surface. Also, the use of imaging techniques such as x-ray tomography¹ or NMR imaging² has been limited to the analysis of structural heterogeneities or of miscible or immiscible diphasic front structures at a scale much larger than the pore size.

However, a thorough understanding of transport in porous media requires that the structure of the velocity field be known at the pore scale: This is necessary, in particular, to detect the existence of low-velocity zones, where the exchange of matter or molecular species with the outside can only take place through molecular diffusion. Such information is of practical relevance to understanding processes such as tracer or pollutant absorption, dispersion in porous media, and filtration. One particularly important issue is the transition between small-scale local processes such as tracer mo-

tion in local velocity gradients and large-scale processes described by the usual transport parameters.

In addition, recent developments in the field of computational fluid mechanics now allow us to obtain precise representations of the three-dimensional (3-D) structure of flow velocity or electrical current fields in simple random porous media.³⁻⁷ They can be used to verify experimental measurements on similar systems by new techniques before the latter are applied to more complex media.

Among the local flow measurement methods already utilized for porous media, some use transparent porous media and matched index fluids: In this case one may use either laser velocimetry techniques⁸⁻¹⁰ or Particle Image Velocimetry.¹¹ Such measurements require either a complex and lengthy 3-D scanning procedure or a careful image analysis, including the determination of a large number of particle trajectories. Also, this approach is limited to transparent media and cannot be extended to real rocks.

Application of NMR imaging to liquid flows in porous media has been reported by Edelstein *et al.*,¹² Majors *et al.*,¹³ and Edwards *et al.*¹⁴ This technique can provide spatial information about matrix porosity and time average displacements of the fluid particles during an observation time Δ ($100 \text{ ms} < \Delta < 1 \text{ s}$ in a typical machine). From such spatial fluid displacement mappings, the probability distribution of the flow velocity in a macroscopic sample volume can be estimated, provided the displacement of the particles is small

^{a)}E-mail: lebon@pmmh.espci.fr

^{b)}Present address: Laboratoire FAST (URA CNRS No. 871), Bât. 502, Campus Université Paris Sud, 91405 Orsay, France.

enough to be proportional to the local velocity.^{15,16} The technique has been, in particular, applied to the estimation of the mean velocity variations near rigid walls bounding an open pore polyurethane foam sample.¹⁷

In this paper, we report a set of measurements carried out in porous media using a pulsed field gradient spin-echo (PFGSE) technique. Such measurements determine quantitatively the distribution of displacement components of the fluid molecules parallel to the field gradient during a predetermined time Δ .^{14,18} At short Δ values for which the pathlength is small compared to the pore size, this gives immediately the distribution of the velocity component parallel to the gradient. In the limit of very long times, such that a large enough number of pores is explored, the distribution of the pathlengths is directly related to the corresponding dispersion coefficient in the medium (longitudinal or transverse depending on the orientation of the field gradient with respect to the mean flow). A key advantage of this method is the fact that the full velocity distribution can be determined at once for all fluid particles located in the measurement volume.

For this paper experiments were performed on unconsolidated monodisperse spherical bead packings fully saturated with flowing water. A first set of measurements allowed us to determine precisely the velocity distribution and to compare it to numerical simulations using the same geometry. Particular care has been given to the analysis of the influence of the flow velocity and of the measurement time on the distribution of the displacements. We have also investigated the influence of pure molecular diffusion on the transport processes. In subsequent experiments, we have studied, at larger time intervals, the distribution of the displacements when these are no longer small compared to the pore size.

II. PULSED FIELD GRADIENT SPIN-ECHO NMR MEASUREMENT TECHNIQUE

A. Experimental NMR setup

Experiments have been performed with a 100 MHz Bruker CXP-100 pulsed NMR spectrometer with a vertical superconducting solenoid, providing a magnetic field $B_0 = 2.35$ T. The flow was studied in a straight circular 10 mm OD glass tube containing the porous medium [for NMR experiments, dielectric materials (glass, ceramics, resin) transparent to the radiofrequency electromagnetic field have to be used]. The tube is placed along the axis of the superconducting solenoid parallel to the magnetic field B_0 . In the center of the solenoid, where the magnetic field B_0 is most homogeneous, a NMR saddle coil is adjusted to the tube. This coil is used to deliver the radiofrequency pulses and to detect the magnetization induction; it defines a measurement volume V of length $L \cong D = 10$ mm inside which the flow is studied. The gradient field pulses are provided by a quadrupole gradient coil wound on a 30 mm diameter macor mandrel of an axis perpendicular to the pipe.¹⁹ Pulsed field gradients of up to 1 T/m oriented along the flow axis are used in the experiments. The height, $2h$, of the superconducting solenoid is approximately 50 cm. In our experiments, the flow

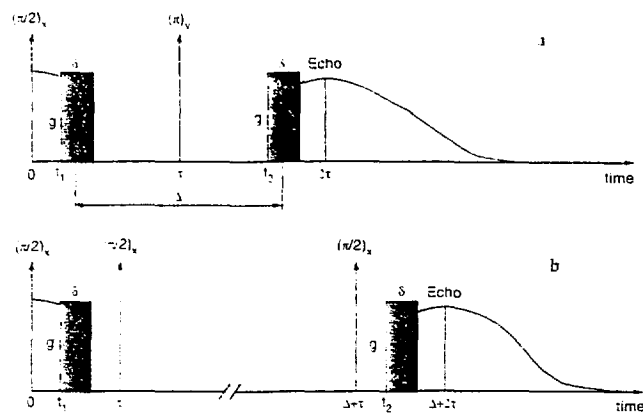


FIG. 1. Pulse sequences used in our experiments. (a) PFG-SE sequence. (b) PFG-SSE sequence.

velocity is always low enough so that the transit time through the measurement volume is much larger than the longitudinal spin relaxation time T_1 .

B. Spin-echo NMR displacement measurements

In the PFG-NMR technique, fluid velocity measurements are performed by superimposing over the constant field B_0 one of the combined rf-magnetic field gradient pulse sequences of Figs. 1(a) and 1(b). We assume that, before each pulse sequence is applied, the magnetization induced by the previous one has relaxed along the direction of the static magnetic field B_0 . Let us turn our attention to a small element (j) of flowing fluid located in the measurement volume V and note $x_j(t)$, $y_j(t)$, $z_j(t)$, its coordinates in the referential (O, x, y, z) [O is the center of the volume V (center of the rf coil) and the z axis is parallel to both the static magnetic field and the field gradient]. During a given sequence, the magnetic field \mathbf{B} on the element is either $\mathbf{B} = \mathbf{B}_0$ without the field gradient, or to $\mathbf{B} = \mathbf{B}_0 + g z_j(t)$ when a field gradient is applied.

Figure 1(a) describes the so-called Hahn echo sequence that has been used in the first part of our experiments.²⁰ We shall refer to it as a PFG-SE sequence (Pulse Field Gradient Spin Echo). First, a $(\pi/2)_x$ rf pulse is applied: It tilts the proton magnetization of the element (j) onto the Y axis in the frame (O, X, Y, Z) , rotating with an angular frequency $\omega_0 = \gamma B_0$ about the Z axis (γ is the gyromagnetic ratio of the proton). During the time interval $(t_1, t_1 + \delta)$, the field gradient g shifts the phase of the magnetization component in the plane (O, X, Y) ; this phase shift is given by

$$\phi_j(t) = \gamma g \int_{t_1}^{t_1 + \delta} z_j(t) dt. \quad (1)$$

Neglecting the displacement of the element (j) in the duration δ of the field gradient pulse [i.e., assuming $\gamma \delta g (dz_j/dt)_{t_1} \ll 1$], one obtains $\phi_j(t_1) = \gamma \delta g z_j(t_1)$.

Then a $(\pi)_y$ rf pulse changes the sign of the phase shift, which becomes $\phi_j(t_1) = -\gamma \delta g z_j(t_1)$.

A second magnetic field gradient pulse applied with the same amplitude and duration at a time t_2 induces another phase shift proportional to the new coordinate $z_j(t_2)$ of the

element. Thus, the resulting phase shift at the time 2τ expected for the echo associated with the refocusing of the signal will be

$$\phi_j(2\tau) = \gamma \delta g [z_j(t_2) - z_j(t_1)]. \quad (2)$$

The magnetization $M(t)$ is the sum of all contributions from the different elements (j) inside the measurement volume V :

$$M(t) = M_0 \langle \exp\{i\phi_j(t)\} \rangle_j, \quad (3)$$

where M_0 is the amplitude of the total proton magnetization in V and $\langle \rangle_j$ is an ensemble average over all elements inside V . The complex amplitude $M_1(2\tau)$ of the first echo may then be written as

$$M_1(2\tau) = M_0 \langle \exp\{i\gamma \delta g [z_j(t_2) - z_j(t_1)]\} \rangle_j. \quad (4)$$

Following Callaghan,²¹ we introduce the probability distribution $P_\Delta(z)$ of the displacements z during the time lapse Δ . Equation (4) can be rewritten as

$$M_1 = M_0 \int P_\Delta(z) \exp[i\gamma \delta g z] dz. \quad (5)$$

The amplitude $M_1(k)$ of the first echo is therefore the Fourier transform of the propagation function $P_\Delta(z)$ in which the wave number $k = \gamma \delta g$ is the variable conjugate to the displacement z . This sequence has been used in all our first experiments but was limited to relatively short measurement times.

Figure 1(b) presents another sequence first introduced by Tanner,²² which allows the use of larger Δ values than the previous one. In this sequence, called PFG-SSE (Pulse Field Gradient-Stimulated Spin Echo), two identical magnetic field gradient pulses are superimposed on a stimulated spin echo sequence. After the first $(\pi/2)_x$ rf pulse tilting the magnetization along the y axis, the first magnetic field gradient pulse encodes the position of every water molecule by a phase shift: $\phi_j(t_1) = \gamma \delta g z_j(t_1)$. The second $(\pi/2)_x$ rf pulse brings back the y component of magnetization into longitudinal polarization along the z axis. Then, after a delay Δ , a third $(\pi/2)_x$ rf pulse tilts back the z component of the magnetization along the y axis and is followed by a second field gradient pulse, which restores partly the phase of each spin through a second shift: $-\gamma \delta g z_j(t_2)$. Thus, the net phase shift at the end of the sequence is $\phi_j(\Delta + 2\tau) = \gamma \delta g [z_j(t_1) - z_j(t_2)]$. Globally, the PFG-SSE sequence provides the same phase shifts as the PFG-SE one: The significant advantage of the technique is the fact that the magnetization remains along the z axis during most of the measurement time. This has two consequences.

(i) The loss of magnetization is no more determined by the transverse relaxation, but by the longitudinal relaxation time T_1 , which is much longer than the transverse relaxation time T_2 .

(ii) The magnetic field deviations due to heterogeneities of the magnetic susceptibility in the porous medium have no effect on the magnetization during the time lapse Δ between the $(\pi/2)_x$ rf pulses.

Practically, the maximum usable time Δ that was about 20 ms for Hahn's sequence (corresponding to displacement of order 60 μm), can be extended to more than 200 ms with

the PFG-SSE technique. Let us note that, for the PFG-SE sequence, one measures the displacement of the fluid particles during the time Δ , while, for the PFG-SSE one, the effective measurement time is $\Delta + \tau$ [τ being the time interval between the two first $(\pi/2)_x$ rf pulses].

C. Effect of the heterogeneities of the magnetic field

Because of the heterogeneities of the magnetic susceptibility in the porous medium, the magnetic field B_z is not homogeneous in the fluid. Thus, each element of fluid is submitted to a magnetic field fluctuation $b(t) = B_z(t) - B_0$ along its trajectory, where $B_0 = \langle B_z \rangle$ is the magnetic field averaged over all the fluid. At time 2τ , for the Hahn sequence, the phase shift of the transverse magnetization of a given fluid particle, due to the heterogeneities of the local magnetic field b , is given by

$$\phi_b(2\tau) = \gamma \int_\tau^{2\tau} b(t') dt' - \gamma \int_0^\tau b(t') dt'. \quad (6)$$

For short values of τ such that the displacement of water molecules is much smaller than the characteristic microscopic length l_c of the porous medium, $b(t')$ is assumed to be constant during τ , so that

$$\phi_b(2\tau) \approx \gamma \tau [b(t_2) - b(t_1)]. \quad (7)$$

Let us note here that this expression of the phase shift at the echo is the same for the stimulated echo sequence. The above assumption is fulfilled in our experiments. The characteristic distance over which magnetic field variations b occur is of order l_c ; thus, for small displacements such that $z \ll l_c$, we have

$$[\phi_b(2\tau)]^2 \ll 2 \gamma^2 \tau^2 \langle b^2 \rangle \approx 1 \text{ rad}. \quad (8)$$

The resulting echo attenuation associated with the variations of the magnetic field b will be the average of $\exp[i\phi_b(2\tau)]$ over all the spins, which, for a Gaussian distribution of phases, is $\exp(-\frac{1}{2}[\phi_b(2\tau)]^2)$. The effect of these variations can be neglected in our measurements because $\langle z \rangle \ll l_c$.

D. Calibration of the applied field gradient for pure diffusion with zero flow

Under zero flow conditions, proton displacements are only due to pure molecular diffusion. Then the probability distribution $P_\Delta(z)$ of the displacements z during Δ predicted by the theory of diffusion is

$$P_\Delta(z) = \frac{1}{\sqrt{2\pi\sigma^2}} \exp\left(-\frac{z^2}{2\sigma^2}\right), \quad (9)$$

in which σ is the mean square deviation of the displacement related to the molecular diffusion coefficient D_0 by $\sigma^2 = 2D_0\Delta$. Equation (9) corresponds to free diffusion in a bulk fluid: It will be valid in the present experimental case in which displacements are very small compared to the pore size so that the structure of the porous medium does not need to be taken into account.

Taking the Fourier transform of $P_\Delta(z)$, the variation with the field gradient g of the amplitude of the first echo measured with the PFG-NMR technique should verify

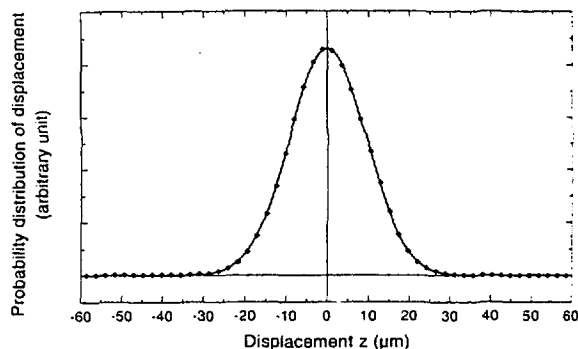


FIG. 2. Probability distribution of the displacement z along the field gradient for a pure molecular diffusion experiment under zero applied flow (PFG-SE experiment, $\Delta=20$ ms, $\delta=2$ ms). The measured distribution (diamond symbols) is very fit accurately by a Gaussian variation (solid line).

$$M = M_0 \exp - [(\gamma g \delta \sigma)^2 / 2]. \quad (10)$$

From the experimental data, one can therefore extract the product $g\sigma$. Thus, Eq. (10) allows us to determine the gradient g from the value of σ ; we routinely use this measurement to calibrate the field gradient g . Figure 2 displays an experimental distribution $P_{\Delta}(z)$ obtained in pure water: We observe that it can indeed be very accurately fit by a Gaussian variation according to Eq. (9).

III. EXPERIMENTAL RESULTS

A. Porous sample preparation

We use as the porous medium an unconsolidated packing of glass beads fitted inside the 8 mm inside diameter of the central tube. The beads have a uniform diameter $d=800 \pm 150 \mu\text{m}$ and the packing is prepared by letting them sediment inside the tube initially filled with water. The length of the porous sample is 10 cm and it is retained by stainless steel grids with a $100 \mu\text{m}$ mesh size; its porosity is of order 0.36. The flow is induced by a constant flow-rate syringe pump with a 100 ml cylinder volume: We used flow rates ranging between 1.5 and 7.3 ml/min: the corresponding interstitial velocities U vary from 1.3×10^{-3} to 6.7×10^{-3} m/s. The corresponding Reynolds number values $\text{Re} = Ud/3\nu$ are between 0.36 and 1.8.

B. Analysis of the experimental data

Figure 3(a) displays a typical variation of the real and imaginary parts of the first echo with the applied field gradient using the PFG-SSE sequence. Each curve typically contains 100 data points and requires an acquisition time of about 160 min. Each data point corresponds to the average of ten independent measurements. The interval between two sequences is of order 10 s representing five times T_1 for protons in pure water. Taking the inverse FFT of the curves of Fig. 3(a), one obtains the probability distribution for the displacement of the water molecules along the direction z of both the field gradient and the mean flow. In order to minimize errors due to the discretization of data, we complement the experimental data points series with zero values up to a total of 512 points; the inverse FFT is calculated from these

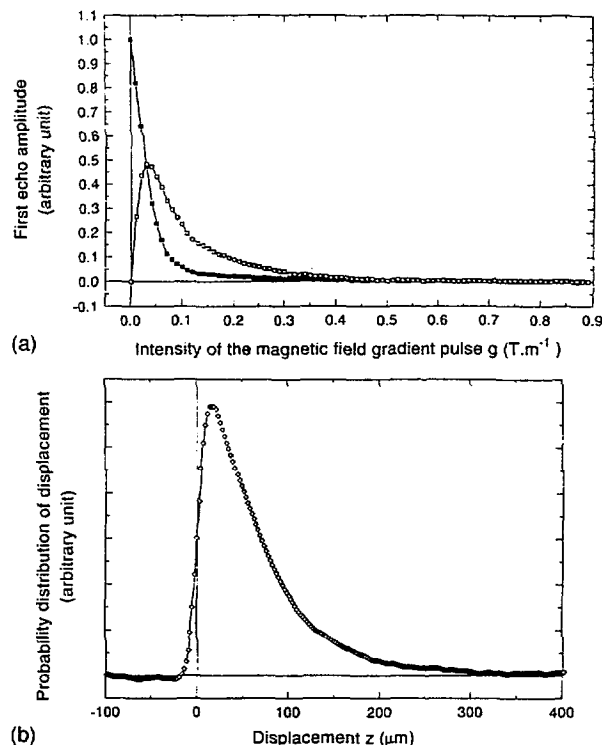


FIG. 3. (a) Experimental variation of the real and imaginary parts (respectively, black and white squares) of the complex amplitude of the first echo obtained in a typical PFG-SSE experiment (experiment #4 in Table I). (b) Fourier transform of the previous curve giving the probability distribution of the displacement z (μm) along the magnetic field gradient (experiment #4, see Table I).

512 points: This is equivalent to a data interpolation in the z space. A typical displacement distribution is shown in Fig. 3(b) for an experiment corresponding to displacements of order $65 \mu\text{m}$, much smaller than the grain size. Table I compares the variations of the mean displacement $\langle z \rangle_{\text{NMR}}$ determined from such experimental curves to the theoretical value $\langle z \rangle_{\text{th}} = Q\Delta/S\phi$ (Q is the global flow rate and S and ϕ are the sample porosity and section). For the PFG-SSE technique, Δ must be replaced by $\Delta + \tau$. Figure 4 displays the variation of $\langle z \rangle_{\text{NMR}}$ as a function of $\langle z \rangle_{\text{th}}$ for all measurements that we have performed: We observe that the two values coincide to within $\pm 5\%$ up to very long mean displacements of roughly $300 \mu\text{m}$.

C. Velocity distributions at short measurement times

As a first step, we used the technique to analyze the probability distribution of the velocity component along the field gradient. For that purpose, we chose Δ values low enough so that the displacement z of the particles is small compared to the pore size. In this case, Eq. (5) may be replaced by

$$M_1 = M_0 \int P(v_z) \exp[i\gamma \delta g v_z \Delta] dz, \quad (11)$$

in which $P(v_z)$ (often called "velocity spectrum") is the probability distribution of the velocity component of the fluid particles along the field gradient and the mean flow

TABLE I. Characteristic parameters of the experiments.

Experiment number	Sequence	Interstitial velocity (cm/s)	Δ (ms)	δ (ms)	τ (ms)	Mean displacement (μm)	$\langle z \rangle_{\text{RMN}}$ (μm)	$\sigma_{\text{Diffusion}}$ (μm)	Re
1	Hahn	0.67	10	2		62.5	54.1	6.5	1.8
2	Hahn	0.34	15	2		48.7	46.9	8.1	0.9
3	Hahn	0.34	15	2		48.7	46.0	8.1	0.9
4	Stimulated echo	0.34	15	2	4	64.6	64.5	9.3	0.9
5	Stimulated echo	0.34	20	2	4	81.6	81.8	10.5	0.9
6	Stimulated echo	0.13	50	1	3	68.9	73	15.6	0.36
7	Stimulated echo	0.34	35	1	3	129	132	13.2	0.9
8	Stimulated echo	0.34	70	0.5	2.5	247	276	18.3	0.9

direction. In Eq. (11), it is assumed that the measurement interval Δ is smaller than the correlation characteristic time τ_v for the velocities of the tracer particles. This implies that the displacement of the fluid particles is small compared to characteristic dimensions of the pores. Let us point out that this dimension will probably not correspond to the aperture of the narrow channels connecting two pores, but rather to their length, which is of the order of the size of the grains or the larger pores. By contrast, in narrow channels the velocity is extremal and remains correlated over a distance comparable to the channel length, which is much larger than the aperture. When these conditions are met, $P(v_z)$ can be determined by taking the inverse Fourier transform of the variation of the complex echo amplitude M_1 with the field gradient g .

At low enough Reynolds numbers, the local flow velocity is related to the pressure gradient by the linear Stokes equation:

$$\frac{1}{\rho} \text{grad } p = \nu \Delta \mathbf{v}, \tag{12}$$

in which ρ is the fluid density and ν is its kinematic viscosity. In this case the local velocity distribution inside the porous medium should remain exactly the same when the global flow rate is varied within a factor proportional to the total flow rate. An important test of the measurement technique will then be to verify that $P(v_z/\langle v_z \rangle)$ is only a function of

the variable $v_z/\langle v_z \rangle$ for a given porous sample ($\langle v_z \rangle$ is the average of the interstitial velocity over the measurement volume, and is computed from the injected flow rate). Let us point out again that we actually measure the components of the particle displacement parallel to the magnetic field gradient and not directly the velocity components: The above assumptions will be valid, provided the size of the measurement volume is large enough to eliminate single pore size effects.

D. Reproducibility of experimental results

In Fig. 5(a), we compare two experimental velocity dis-

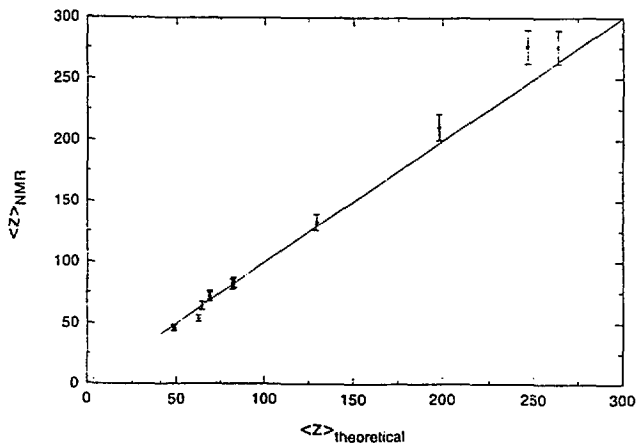
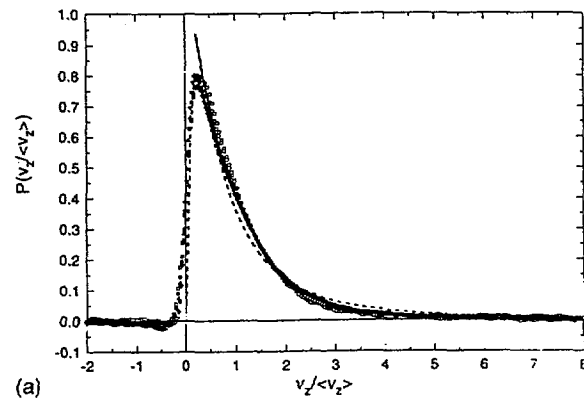
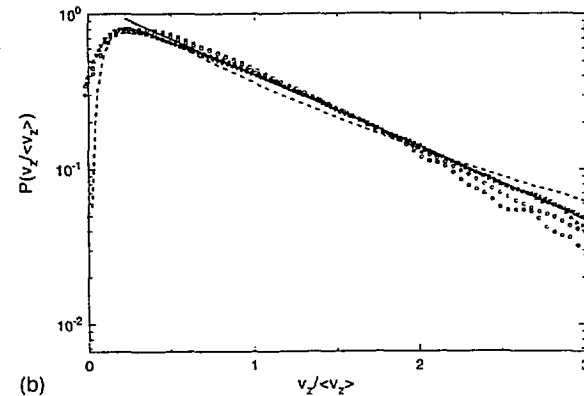


FIG. 4. Variation of the experimental mean displacement $\langle z \rangle$ as a function of the theoretical value $Q\Delta/S\phi$.



(a)



(b)

FIG. 5. (a) Analysis of the reproducibility of the velocity distribution curves and comparison between the PFG-SE and PFG-SSE sequences: The symbols represent different experiments (square: experiment #2, circle: experiment #3, up triangle: experiment #4, down triangle: experiment #5, see Table I); the solid line is an exponential fit, the dashed line a lognormal fit. (b) Shape of the velocity distribution (logarithmic plot).

tributions obtained with a PFG-SE sequence and corresponding to the same measurement times and flow velocities. The other curves correspond to measurements using the PFG-SSE technique for similar experimental parameters. All three curves have been normalized to have an integral equal to 1 and the horizontal scale has been normalized by the mean theoretical velocity (Table I gives the characteristic parameters of these experiments). We observe that all curves coincide quite well and that the normalization compensates well the 70% difference between the mean displacements in the first two curves and in the last one. Let us point out that the global integral of the curves of Fig. 5(a) is very sensitive to the choice of the baseline: Therefore, a small error on the latter induces significant variations of the maximum amplitude. Overall, the maximum amplitude and the mean square width of the distribution are reproducible, with an uncertainty of $\pm 5\%$. This demonstrates that, for displacements small compared to the pore size, the two types of pulse sequences we have used give identical results within the experimental reproducibility that we have tested for the Hahn sequence.

E. Shape of the velocity probability distribution

From their experiments, Cenedese and Viotti¹¹ suggested a lognormal density distribution for the longitudinal velocity in the porous sample they studied (glass cylinders packing), while Georgiadis *et al.*¹⁵ reported an exponential decay of the distribution for high velocities in a spheres packing. Figure 5(a) shows the normalized results $P(v_z/\langle v_z \rangle)$ for different experiments and their approximation by a lognormal and an exponential function. The lognormal function is consistent with the experimental data near the peak, but the decay is better represented by an exponential function for relative velocities $v_z/\langle v_z \rangle$ greater than 0.5: Fig. 5(b) displays $\ln[P(v_z/\langle v_z \rangle)]$ as a function of $v_z/\langle v_z \rangle$. This latter result is in qualitative agreement with that of Georgiadis *et al.*,¹⁵ who also found an exponential decay of the velocity distribution; the difference observed in the low-velocity part of the curve may be due in part to differences of the packing structure. It may also be associated with the different procedures used for determining this curve: In our setup we obtain directly an average over the full measurement volume, while, in the imaging experiment, the curve must be obtained from a discrete set of values corresponding to each voxel of the image.

The lognormal and the exponential function chosen for the approximations are

$$P\left(\frac{v_z}{\langle v_z \rangle}\right) = A \exp\left(-\frac{[\ln(v_z/\langle v_z \rangle)/v_0]^2}{2\sigma^2}\right);$$

$$P\left(\frac{v_z}{\langle v_z \rangle}\right) = B \exp\left(-\frac{v_z/\langle v_z \rangle}{v_c}\right), \quad (13)$$

with $A \approx 0.80$, $v_0 \approx 0.25$, $\sigma \approx 1.1$, $B \approx 1.2$, and $v_c \approx 0.93$. Because of the normalization, all these values are dimensionless.

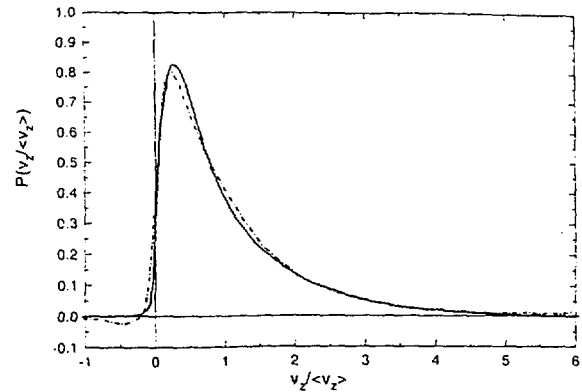


FIG. 6. Comparison between numerical simulations (solid line) and experiments (dashed line: experiment #5, see Table I).

IV. NUMERICAL SIMULATIONS

A. Numerical model porous media

A model porous medium was constructed by dropping, one at time, equal size spheres into a parallelepipedic box from a random location located above the packing. Each new sphere is assumed to come to rest, either when it hits the box floor or when it comes to a stable resting point in contact with three other spheres. Periodic boundary conditions are assumed in the direction transverse to the pressure drop applied in the simulation. Once the center of each sphere has been determined, a digital image of the porous medium is created such that each sphere had a diameter equal to seven units of lattice spacing. The total system size is $157 \times 139 \times 139$: This resolution is high enough so that the narrowest channels are about one to two lattice sites in width. This is a conservative estimate, in that these are relatively rare due to the randomness of the packing.

B. Flow simulation

In order to determine the local flow velocities, we solve Stoke's equation using finite difference methods, in conjunction with the artificial compressibility relaxation algorithm.^{4,5,23} A staggered marker and cell (MAC MESH) was used to represent the pore space and solid regions. Here, pressures are defined at the nodes and the velocities are defined at the center of bonds connecting the nodes. Each voxel, a unit cube assumed to be entirely solid or pore space, is centered at the nodes. We assume that the fluid is incompressible and that the flow velocity is zero along the pore/solid interface (no slip boundary condition). Near the pore/solid interface, noncentered difference equations are used to obtain an accuracy of at least second order and to force the fluid velocities to zero at the interface.

Flow velocity data along the direction of the applied pressure gradient was binned to obtain the distribution function, as seen in Fig. 6. For comparison we superimposed one of our experiments: We observe that flow distributions agree quite nicely; the differences are of the same order as the experimental uncertainties discussed above. Let us note here that the simulated velocity distribution also presents an exponential decay at long velocity.

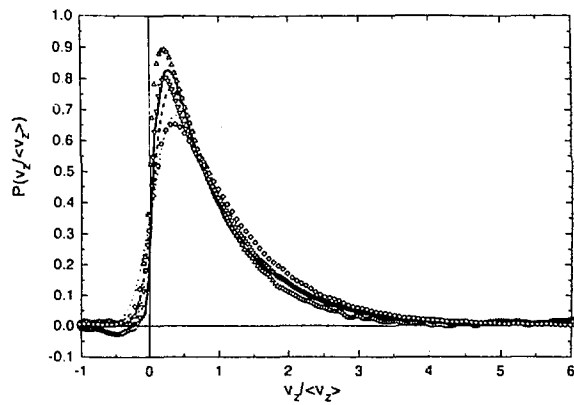


FIG. 7. Estimation of the influence of pure molecular diffusion and of the Reynolds number on the longitudinal displacement distribution: up triangle: experiment #1 ($Re=1.8$, $\Delta_{dir}=12$ ms), down triangle: experiment #5 ($Re=0.9$, $\Delta_{dir}=24$ ms), diamond: experiment #6 ($Re=0.9$, $\Delta_{dir}=53$ ms) (see Table I); convolution of the simulation data by a Gaussian diffusion for typical measurement times in our experiments: The solid line is the simulation data, the dashed line is the simulation data convoluted with a diffusion time of 24 ms, and the dotted line is the simulation data convoluted with a diffusion time of 53 ms.

V. INFLUENCE OF REYNOLDS NUMBER AND MOLECULAR DIFFUSION

In order to determine the Stokes flow velocity distribution in the porous medium from our NMR measurements, two conditions must be met.

(a) The Reynolds number must be low enough so that nonlinear terms in the Navier–Stokes equation of motion of the fluid are everywhere negligible.

(b) The measurement time must be long enough so that the spreading associated with molecular diffusion is negligible compared to the convective displacement by the fluid velocity. The measurement may indeed be perturbed by molecular diffusion both parallel and transverse to the flow lines (the latter may induce additional spreading when a velocity gradient is present). Let us estimate these two effects and compare them to a typical convective spreading. The spreadings due to convection and pure longitudinal molecular diffusion over a time t are, respectively, of order Ut and \sqrt{Dt} . The diffusion distance transverse to the flow lines is also of order \sqrt{Dt} ; in addition, if U is the typical fluid velocity, the transverse velocity gradients are of order U/d . Therefore the corresponding velocity variations are of order $U/d\sqrt{Dt}$, giving a typical spreading distance $U/d\sqrt{Dt^3}$ (in the limit of very long times for which the transverse diffusion distance is of the order of the width of the microscopic flow channels, this mechanism becomes similar to Taylor dispersion).

From these evaluations, one finds first that the ratio of the spreading lengths due to transverse and longitudinal molecular diffusion is of order Ut/d . The former should therefore be negligible as long as the displacement of the particles during the measurement time is small compared to the pore size. On the other hand, the ratio of the gradient assisted molecular diffusion ($U/d\sqrt{Dt^3}$) and convection (Ut) spreading terms is constant with respect to velocity and of order \sqrt{Dt}/d : It will be less than unity, provided that the

measurement time is small compared to the diffusion time d^2/D over a distance of the order of the pore size. This condition will always be fulfilled with the large pores that we are using. The only remaining term that may influence the relation between the velocity distribution and the displacement distribution is the longitudinal molecular diffusion parallel to the flow lines.

We analyzed its effect by plotting in Fig. 7 three experimental velocity distribution curves with similar mean displacements of the fluid particles and Re and Δ values varying by a factor of 5; the corresponding values of the Reynolds number and the expected longitudinal diffusive spreading distance are listed in Table I. We observe that the differences between the three curves are more important than the experimental reproducibility errors displayed in Fig. 5(a): the maximum of the normalized velocity distribution decreases by roughly 30% when the velocity decreases five-fold. The slope of the curve near the zero velocity point is also much smoother. The curves corresponding to the two smallest Reynolds numbers (both <1) are the most different: This implies that longitudinal molecular diffusion is in this case a significant perturbation, since the Stokes approximation should be well verified in both cases. On the contrary, we verify that the two highest velocity curves are more similar: This implies that finite Reynolds number effects were small, since they should be strongest for the $Re=2$ curve.

In order to analyze more quantitatively the influence of longitudinal molecular diffusion on the displacement distribution curves, we have estimated this effect by a convolution procedure. The experimental curve #1 corresponding to the shortest measurement times has been convoluted with a Gaussian representing the pure diffusive spreading of the tracer: This is equivalent to neglecting the additional dispersion due to diffusion across the transverse velocity gradients. The diffusion times have been chosen equal to the difference between the measurements times for experiment #1 and for experiments #5 and #6, respectively. The comparison between these estimations and the latter experimental curves are displayed in Fig. 7. We observe that these estimations predict a sizable broadening of the curves, although smaller than that actually observed: The difference between these estimates may be due to the fact that the displacement is not small enough compared to the pore size and that the term associated with the transverse velocity gradient may be larger than expected. The finite Reynolds number value may also play some role but is quite difficult to compute quantitatively.

VI. DISPLACEMENT DISTRIBUTIONS AT LONGER MEAN DISPLACEMENTS

When the measurement time and/or the flow velocity is increased, the displacement of the fluid particles is not negligible compared to the grain and pore size. The limiting regime, at very long measurement times, corresponds to a classical dispersion process, and would only be reached after the fluid particles have explored a sufficiently large number of pores. In this case, the distribution of the displacements with distance would be a Gaussian curve centered at displacement values corresponding to the mean flow velocity:

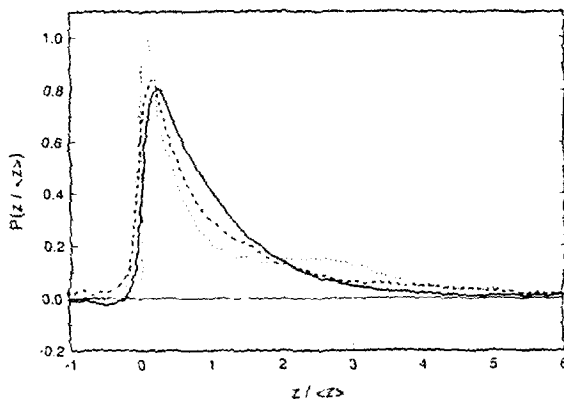


FIG. 8. Comparison of the displacement distributions observed for longer measurement times (dashed line: experiment #7, $\langle z \rangle = 130 \mu\text{m}$ and dotted line: experiment #8, $\langle z \rangle = 247 \mu\text{m}$) and a shorter one (solid line: experiment #5, $\langle z \rangle = 81.6 \mu\text{m}$) at the same velocity (see Table I).

The width of the distribution would be directly related to the effective dispersion coefficient in the medium. Such large distances have not been reached in our experiments; however, we obtained experimental curves corresponding to the transition domain, in which the mean displacement is of the order of the pore size.

Figure 8 represents distributions corresponding to mean displacements $\langle z \rangle = 129$ and $247 \mu\text{m}$ (about two-thirds of the radius of the glass beads) and to measurement times $\Delta t = 38$ and 72.5 ms, a curve corresponding to a smaller mean displacement $\langle z \rangle = 82 \mu\text{m}$ has been superimposed for comparison. Such measurements are only possible with the PFG-SSE technique. We observe that the relaxation of the distribution of displacements is no longer exponential in the region $\langle z \rangle < z < 4\langle z \rangle$, and that the part of the curve corresponding to $z/\langle z \rangle > 2$ is well above that obtained in previous measurements. The curve $\Delta t = 72.5$ ms presents a second peak for $z/\langle z \rangle \approx 2.5$: It may be a precursor of a dispersion peak and is associated with faster moving particles. The curve $\Delta t = 38$ ms has an intermediate shape with an inflection point instead of a second peak. At longer mean displacements, one should obtain a unique dispersion peak, as observed by Edwards *et al.*¹⁴

VII. CONCLUSION

In the present paper, we have analyzed at a very local scale the displacement of fluid particles due to flow inside a porous medium, using both a pulsed NMR technique and numerical simulations. Using proper stimulated spin-echo sequences, long mean displacements of up to $250 \mu\text{m}$ corresponding to measurement times of up to 200 ms can be analyzed: The measured values are in good agreement with direct computations from the sample porosity and the injected flow rate. An important issue determining the range of use of the technique will be the influence of magnetic permeability heterogeneities on the measurement, particularly when real rocks and smaller pore sizes will be used. In the present experiments, $800 \mu\text{m}$ diameter glass beads were used and such effects did not appear to be significant.

At displacements much smaller than the pore size, one obtains directly the distribution of the velocity components along the pulsed magnetic field gradient chosen parallel to the mean flow. Outside of cumbersome optical determinations in transparent media, no other experimental technique allows one to obtain such information that may be very useful to analyze transport in porous media and detect heterogeneities. At low velocities, the effect of longitudinal molecular diffusion parallel to the mean velocity may be significant, and must be corrected. At higher velocities, the displacement distribution is extremely similar to that obtained from simulations in which the Stokes equation is directly solved in the geometry of a random packing of spheres constructed numerically. An interesting feature of these distributions is to display an exponential relaxation at long distance: They deviate markedly from the lognormal distribution measured by other authors. The probability distribution takes large values for low velocities much below the mean value, but few molecules appear to have a negative velocity: This result should be compared to measurements in more heterogeneous media (sintered glass beads, for instance), for which a larger number of flow channels may display velocity components opposite to the mean flow. Velocity distribution variations due to deviations from the Stokes regime did not appear clearly even at a Reynolds number $Re = 2$: Still higher flow velocities should probably be investigated. The interplay between molecular diffusion and nonlinear effects may also be usefully investigated using higher viscosity fluids.

At longer displacements of the order of the pore size, strong distortions of the overall shape of the displacement distribution are observed. These distortions appear to indicate the onset of the transition toward a classical dispersion regime that should take place when the fluid particles explore a large number of pores during the measurement time. In this case, the tracer corresponds simply to the spin of particles excited by the NMR pulses and follows perfectly the local fluid flow in contrast with practically all usual tracers. No other dispersion measurement technique allows such measurements at a very local scale. A secondary peak corresponding to the fastest particles was clearly observed at the largest displacement values that we used: At larger displacement distances, one expects a reduction of the low-velocity part of the distribution and an increase of such a peak as well as a drift toward the mean velocity. One way to further analyze this transition is to use a porous packing obtained using smaller grains.

In conclusion, using sophisticated pulse sequences allows us to measure displacements of several hundred μm . Pulse field gradient NMR then becomes a very flexible and unique tool for analyzing velocity distributions and spatial correlations at a length scales ranging from approximately 1 – $300 \mu\text{m}$. Of particular importance is the fact that we obtain the full distribution of a given displacement component in a single measurement. Future work is needed to demonstrate the feasibility of such measurements in a broader range of natural and artificial media.

¹⁴F. M. Auzerais, D. V. Ellis, S. M. Luthi, E. B. Dussan, and B. J. Pinoteau, "Laboratory characterization of anisotropic rocks," SPE Paper No. SPE

- 20602, presented at the 65th annual conference and exhibition of the Society of Petroleum Engineers, New Orleans, LA, 23–26 September 1990.
- ²G. Guillot, C. Chardaire-Rivière, S. Bobroff, A. Le Roux, J. C. Roussel, and L. Cuic, "Characterisation of wetting heterogeneities in sandstone rocks by MRI," *Mag. Reson. Imag.* **12**, 365 (1994).
- ³N. Martys, "Fractal growth in hydrodynamic dispersion through random porous media," *Phys. Rev. E* **50**, 335 (1994).
- ⁴L. M. Schwartz, N. Martys, D. P. Bentz, E. J. Garboczi, and S. Torquato, "Cross property relations and permeability estimation in model porous media," *Phys. Rev. E* **48**, 4584 (1993).
- ⁵N. Martys and E. J. Garboczi, "Length scales relating the fluid permeability and electrical conductivity in random two-dimensional model porous media," *Phys. Rev. B* **46**, 6080 (1992).
- ⁶P. M. Adler, C. G. Jacquin, and J. F. Thovert, "The formation factor of reconstructed porous media," *Water Res. Res.* **28**, 1571 (1992).
- ⁷J. Salles, J. F. Thovert, and P. M. Adler, "Reconstructed porous media and their application to fluid flow and solute transport," *J. Contaminant Hydrology*, **3**, 3 (1993).
- ⁸A. Dybbs and R. V. Edwards, "New look at porous media fluid mechanics," Darcy to turbulent in *Fundamentals of Transport Phenomena in Porous Media*, edited by J. Bear and M. Y. Corapcioglu (Martinus Nijhoff, Dordrecht, 1984), pp. 201–256.
- ⁹A. Dybbs and R. V. Edwards, "An index matched flow system for measurements of flow in complex geometries," *4th International Symposium on the Applications of Laser Anemometry to Fluid Mechanics*, Lisbon, 1988.
- ¹⁰R. L. Varty and I. G. Currie, "Index-matched laser-anemometer measurements of cross-flow in tube bundles," in Ref. 9.
- ¹¹A. Cenedese and P. Viotti, "Lagrangian analysis of non reactive pollutants dispersion in porous media by means of a PIV technique," preprint, 1994.
- ¹²W. A. Edelstein, H. G. Vinager, P. N. Tutujian, P. B. Roemer, and O. M. Mueller, "NMR imaging of core analysis," *Proceedings of the 63rd Annual Technical Conference and Exhibition*, Society of Petroleum Engineers, SPE 18272, 101–112, 1988.
- ¹³P. D. Majors, J. L. Smith, F. S. Kovarik, and E. Fukushima "NMR spectroscopic imaging of oil displacement in dolomite," *J. Magn. Res.* **89**, 470 (1990).
- ¹⁴C. M. Edwards, C. T. Chang, and S. Sarkar, "The measurement of fluid velocities in porous media," SCA Conference Paper No. 9310, 1993.
- ¹⁵J. Georgiadis, R. Behringer, M. Shattuck, and G. A. Johnson, "Interstitial velocity and temperature fields in fully-saturated porous media," *9th Symposium of Energy Engineering Sciences*, Fluid and Dynamical Systems, 1991.
- ¹⁶M. Schattuck, R. Behringer, J. Georgiadis, and G. Johnson, "Magnetic resonance imaging of interstitial velocity distribution in porous media," in *Experimental Techniques in Multiphase flows*, ASME Proceedings, edited by O. Hern and R. Gore, New York, 1991, Fed-Vol. 125, pp. 39–46.
- ¹⁷L. C. Givler and S. A. Altobelli, "A determination of the effective velocity for the Brinkman–Forcheimer flow model," *J. Fluid Mech.* **258**, 355 (1994).
- ¹⁸P. T. Callaghan, *Principles of Nuclear Magnetic Resonance Microscopy* (Clarendon Press, Oxford, 1991).
- ¹⁹D. S. Webster and K. H. Marsden, "Improved apparatus for the NMR measurement of self-diffusion coefficients using pulsed field gradients," *Rev. Sci. Instrum.* **45**, 1232 (1974).
- ²⁰E. O. Stejskal and J. E. Tanner, "Spin diffusion measurements: Spin echoes in the presence of a time-dependent field gradient," *J. Chem. Phys.* **42**, 288 (1965).
- ²¹P. T. Callaghan, "Pulsed field gradient nuclear magnetic resonance of liquid state molecular organization," *Austr. J. Phys.* **37**, 359 (1984).
- ²²J. E. Tanner, "Use of the stimulated echo in NMR diffusion studies," *J. Chem. Phys.* **52**, 2523 (1970).
- ²³R. Peyret and T. D. Taylor *Computational Methods for Fluid Flow* (Springer-Verlag, New York, 1983).

